Investigation of sulphate origins in the Jeffara aquifer, southeastern Tunisia: A geochemical approach

SAMIR KAMEL*, MOHAMED BEN CHELBI and YOUNES JEDOUI

Institut Supérieur des Sciences et Techniques des Eaux de Gabès, Cité Erriadh. Campus Universitaire, Zrig. Gabès 6072, Tunisia.
Corresponding author. e-mail: samir.kamel@isstegb.rnu.tn

The chemical composition of groundwater within the multilayer Jeffara aquifer and the detailed analysis of saturation indices enables identification of the origin of mineralization and hydrogeochemical processes occurring in groundwater. It has been demonstrated that groundwater is mainly characterized by a Ca–Mg–SO$_4$–Cl water type. Geochemical pattern is controlled by the dissolution of evaporites, largely abundant in the study area and incongruent dissolution of dolomite. Gypsum, anhydrite, mirabilite and thenardite have been examined as potential sources of sulphate dissolved in groundwater. Since Jeffara groundwater is recharged by the Continental Intercalaire (CI) geothermal water, water temperature decreases from the CI to the Jeffara aquifer. Solubility of the majority of minerals is modified by this change in temperature and thus a mixing process of thermal and non-thermal waters was examined.

1. Introduction

Water analyses carried out in the Jeffara basin provide an opportunity to recognize the relationship between evaporites bearing different sedimentary rocks and a mechanism that leads to the salinization of groundwater.

The Jeffara basin is the largest, coastal type basin in central North Africa, and shared between Tunisia and Libya. It covers about 15,000 km² drainage area running from southeast Tunisia, near Gabes, to north–west Libya, east of Tripoli and declining gradually, towards the Mediterranean Sea. The present study is focused on the northern part of the Jeffara plain known as 'the Jeffara of Gabes' (figures 1 and 2).

Jeffara basin encloses numerous sebkhas (saline lakes), but they are progressively drained by the expanded cities. Gypsum is by far the most abundant calcium sulphate mineral that forms under normal sedimentary conditions (Kinsman 1966). Indeed, it occurs in the study area, in different forms:

(1) Alternating with dolomite, marl and gypsum in subsiding deposit up to 800 m thickness in northern Chott Chain (figure 1).
(2) Interbedded in massive and compact deposit of terraces. In the case where erosion affected the upper part of the terrace, gypsum increased more consistently and changes in gypsum crust were observed (Swezey 2003). These gypsum layers of one to several metres thickness, in the deposits forming the terraces, were marked on the banks of Sourag, Zerkine Wadis and in the Oum Zessar and Zerkine Sabkhat (figure 1).

In southern Tunisia, thousands of exploration and development oil boreholes have identified an
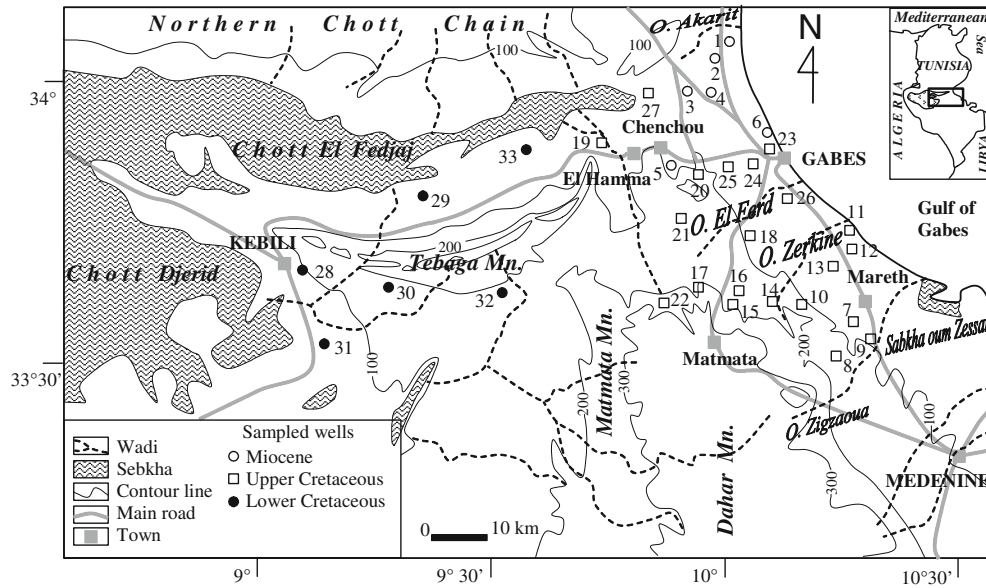
Figure 1. Study area in south-eastern Tunisia with geographic features and location of sampled wells. Jeffara plain is surrounding by low reliefs not exceeding 500 m height and the Saharan desert with large chotts.
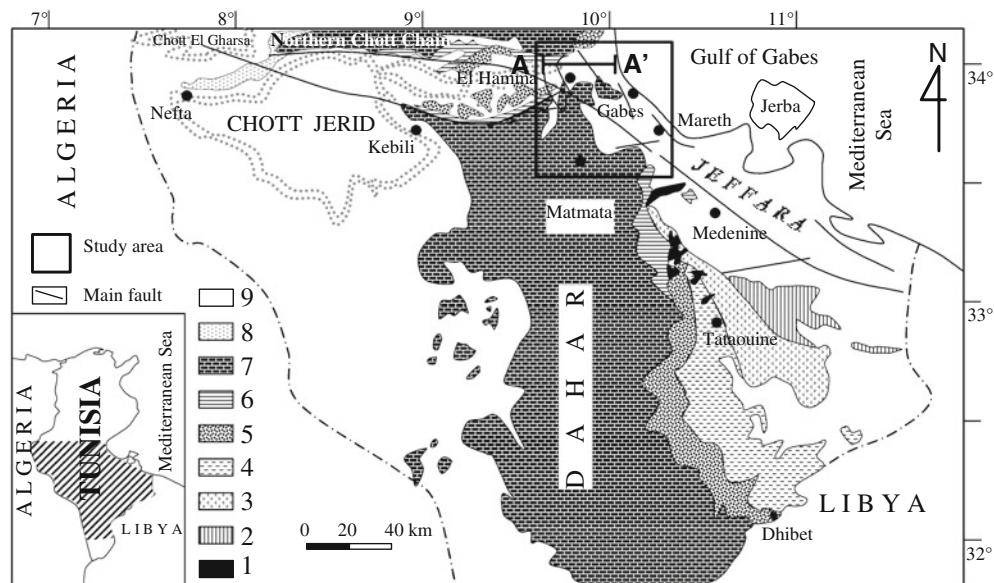

Figure 2. Simplified geological map (after Benton *et al.* 2000) with cross-section AA′ location 1: Permian, 2: Triassic, 3: Lias, 4: Dogger, 5: Malm, 6: Vraconian (mid-late Albian), 7: Late Cretaceous, 8: Mio-Pliocene, and 9: Pliocene–Quaternary. The evolution of outcrops age is from southeast to northwest.

important evaporitic formation (gypsum/anhydrite) related to deposits of Upper Triassic–Lower Jurassic (Bir Ghanem Formation), Upper Jurassic (Abreghs Formation) and to the Lower Cretaceous ages (Zeggab Formation) (Mamou 1990; Bouaziz 1995).

The Gabes region is characterized by arid to semi-arid climate influenced by dry and hot air masses coming from the desert and by humid air masses coming from the Mediterranean Sea (Mekrazi 1975). Precipitation is rare and irregular, occurring mostly from October to January. The annual average precipitation is of 189 mm and mean annual temperature is 21°C. The drainage network consists of the non-perennial Wadis which collects runoff water from the northern Chott Chain, Matmata and Dahar range. Potential evapotranspiration is about 2760 mm per year

(Abidi 2004) and most of the rainwater is lost by evaporation.

Available surface water is insufficient for current domestic, industrial and agricultural needs of the region. Consequently, groundwater constitutes the main water resource in the Jeffara plain.

About 86% of Jeffara of Gabes total domestic, industrial and agricultural water demands, estimated as 104 million m³/year, is covered by groundwater abstraction (DGRE 2009). Original conditions were those of a fully saturated artesian basin even some 100 years ago with numerous springs occurring across the plain.

Hundreds of shallow and more than 500 deep wells were drilled to meet the rapidly growing demand for water (Abidi 2004).

Earlier work carried out in the Jeffara plain consists of hydrochemical and statistical studies (Kettata *et al.* 2009) and quantification of regional groundwater flow between continental Intercalaire (CI) and Jeffara aquifers using stable isotope balance (Trabelsi *et al.* 2009). There has been limited attempt to study the mechanisms that contribute to water mineralization. Hence, the main objective of this study is to integrate major and minor ion geochemistry with the saturation state of the evaporites in order to identify both the hydrochemical processes and sulphate sources, in the Jeffara aquifer.

Special attention is paid to the behaviour of the hydrated and anhydrous evaporites under the progressive cooling water of the geothermal CI regional flow during its ascent, recharging the Jeffara groundwater. Influence of ascending inflow of water from the geothermal CI recharging the Jeffara aquifer and its cooling along the flow was considered.

2. Study area

The study area is located in the southeastern part of Tunisia and lies approximately between longitudes 9°30′ to 10° 30′ E and 33°30′ to 34° N. It extends from the Mediterranean Sea coast in the east to the Matmata and Dahar in the west, which is the mountain range separating plain of the Jeffara from the Saharan desert. The study area is limited in the north by the northern Chott Chain. The southern limit is constituted by Zigzaoua Wadi, near Mareth city (figure 1).

3. Geology

A simplified geological map of southern Tunisia and a representative lithostratigraphic chart are shown in figures 2 and 3, respectively. Geology of the Jeffara plain consists of a sedimentary succession extending from Permian to Quaternary, with sedimentary gaps from Paleocene to Eocene and during the Lias stage (Mamou 1990). The continental formations of Lower Cretaceous (Neocomian, Barremian, Aptian and Albian) contain the CI, which is located in the Chott el Fedjej and Kebili regions, western part of the study area (figure 1).

In the Jeffara of Gabes, the Upper Cretaceous is represented by the Cenomanian, the Turonian and the Lower Senonian, which is divided into two distinct entities: the marl/gypsum Senonian and the limestone Senonian (Rouatbi 1967). Mio-Pliocene is formed by continental material; gypsum marl and sands.

Quaternary is represented by the Lower Villafranchien–Pleistocene, the Upper Pleistocene and the Holocene (Ben Ouezdou 1983). It is mainly formed by conglomerates, marl and gypsum, which generally repose uncomfortably on the Senonian limestone (Mhamdi *et al.* 2011).

The Jeffara basin has undergone a complex and polyphase structural history since the Carboniferous (Ben Ayed 1986). It has been affected by multiple episodes of tectonism, including a late Paleozoic collision with Laurasia and subsequent early Mesozoic rifting associated with the opening of the Tethyan Ocean (Gabtni *et al.* 2006). Caledonian (Devonian), Hercynian (Carboniferous), Austrian (Early Cretaceous) and Alpine (Late Cretaceous–Early Eocene) on the Jeffara area has been the production of a large sedimentary basin. During Mesozoic extensional tectonics, there was an episode of northwestward tilting of the region, resulting in the superposition of a pre- and post-tilting Mesozoic basin on eroded remains of the Paleozoic basin. The alpine orogeny affected the basin with less intensity than it did in the Atlas Mountains to the north; however, several Hercynian-aged normal faults were locally inverted (Gabtni *et al.* 2006).

4. Hydrogeology

This study is focused on southern Tunisia which forms a part of the northern Saharan sedimentary basin which contains two important aquifer systems extending over an area of 780,000 km² (Guendouz *et al.* 2003): The CI is overlain by the Complexe Terminal (CT). Lateral continuation of the CT in the coastal plain of Tunisia and Libya forms the Jeffara aquifer (OSS 2003). Although lithologically similar, the Jeffara and CT aquifer systems are hydrogeologically and geochemically independent with distinct recharge mechanism and sources, groundwater flow, recharge sources and chemistry (Trabelsi *et al.* 2009).
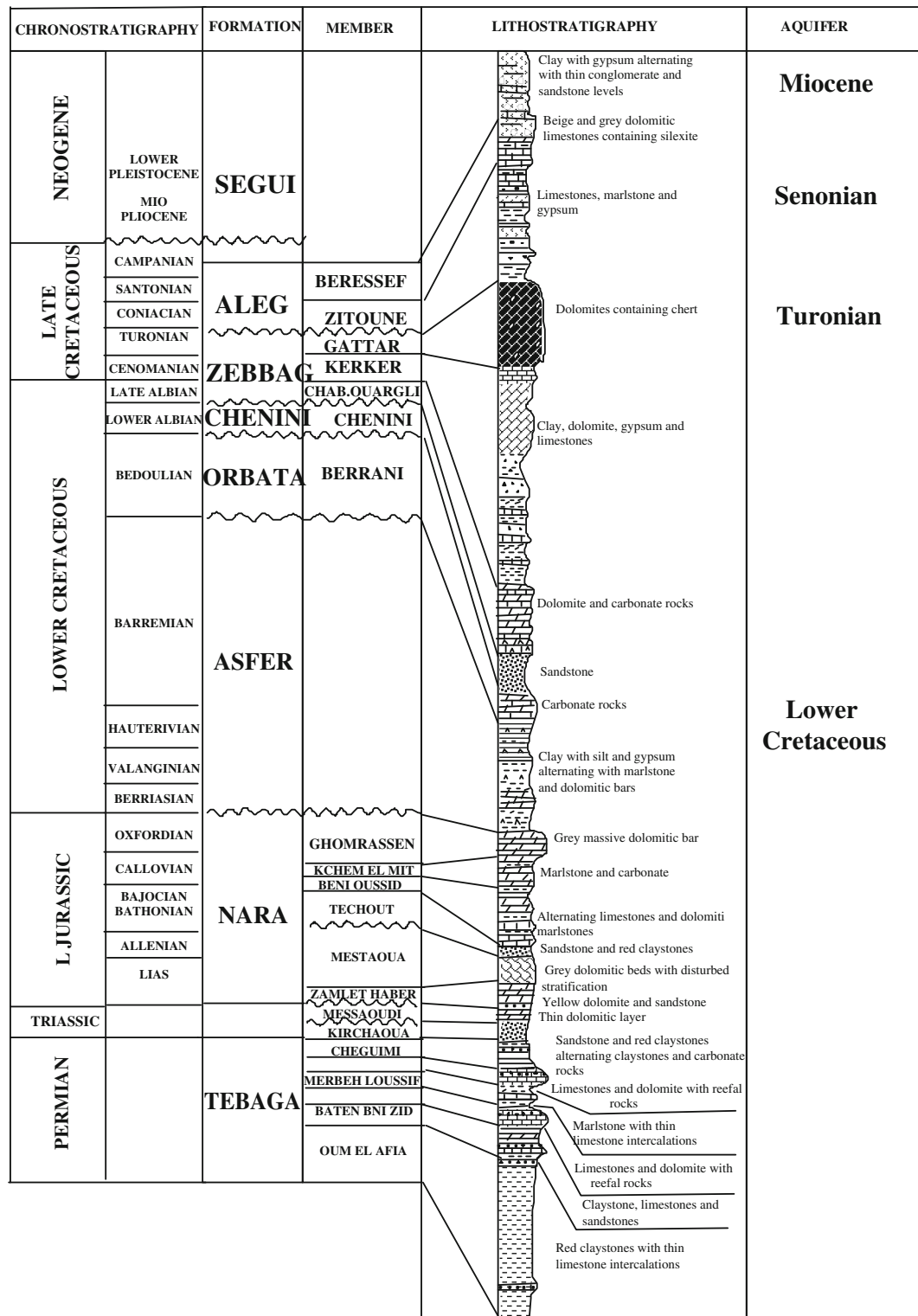
Figure 3. Lithostratigraphic column of southern Tunisia (modified after Mhamdi *et al.* 2011). Miocene and the Lower Cretaceous aquifers are hosted in sandy formation, the Upper Cretaceous aquifer, in fissured limestone. All are associated with gypsum layers.

Numerous geologic and hydrological studies carried out in southeast Tunisia (Rouatbi 1967; Ben Baccar 1982; Mekrazi 1975; Bouaziz *et al.* 2002; Abidi 2004; Kettata *et al.* 2009; Trabelsi *et al.* 2009) have been important in defining the architecture of the Jeffara and boundaries of the potential reservoir. From a structural point of view, the area is represented by horst and graben
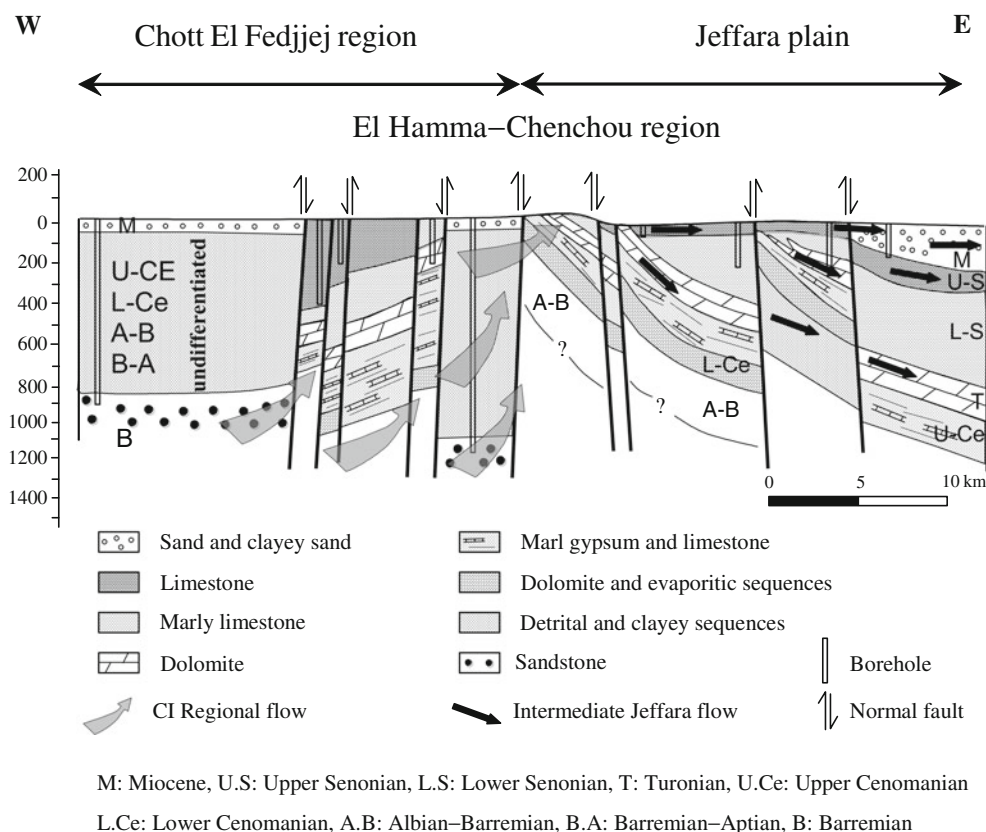
Figure 4. Hydrogeological cross-section AA′, as indicated in figure 2, showing the main flow from CI recharging the Jeffara aquifer.

structures with a distensive tectonic style generated during the Cretaceous. In southern Tunisia, the general tectonic lineament strikes NW–SE with conjugated NE–SW faults that lead to the discharge of CI hot water in the Jeffara aquifer (Bouri *et al.* 2008).

The Jeffara aquifer system is characterized by the variability of lithology and thickness of water-bearing horizons. From the bottom to the top, three hydrostratigraphic units are distinguished (figure 4).

4.1 *The Turonian aquifer*

The Turonian carbonates constitute the principal water-bearing formation in the region of Matmata, El Hamma and Chenchou. The aquifer consists of dolomites and fissured limestones, whose thickness does not exceed 50 m (Rouatbi 1967) (figure 3). Although, its extent is limited, the Turonian aquifer is characterized by high transmissivity, generally around 0.1 m²/s, exceptionally reaching 1.2 m²/s in the Chenchou area where the crustal deformation is particularly intense. The Jeffara basin is strongly affected by tectonism, which

links three different water-bearing horizons into a single hydraulic structure (figure 4).

4.2 *The Senonian aquifer*

The principal aquifer of Gabes consists of Senonian limestone which is abstracted by a large number of boreholes. The Senonian formation consists of two stratigraphic units. The lower one, formed by marl and gypsum, with a thickness of approximately 50 m, is known as 'horizon B'. This level is covered by a limestone level (horizon A) characterized by a variable thickness, up to 500 m (figures 3 and 4). These water-bearing formations are strongly fissured, with the transmissivity ranging from 0.9 10^{-3} to 345 10^{-3} m²/s. All water-bearing formations of the Jeffara plain are hydraulically connected through the existing faults.

4.3 *The Miocene aquifer*

The part of Jeffara aquifer located in northern Gabes (figure 4) is formed by Miocene continental

Table 1. *Physico-chemical data of groundwater.*

Map no.	Formation	pH	T (°C)	C (mS/cm)	TDS (mg/l)	Ca (mg/l)	Mg (mg/l)	Na (mg/l)	K (mg/l)	Cl (mg/l)	SO$_4$ (mg/l)	HCO$_3$ (mg/l)	Sr (mg/l)
1	Sand	7.34	24	5640	3890	349	177	565	38	841	1688	139	5.46
2	Sand	7.23	24	6160	4490	384	165	765	38	927	1967	137	7.61
3	Sand	7.20	23	4610	3320	352	175	490	37	684	1330	129	6.83
4	Sand	7.56	28	5570	4030	416	138	610	38	830	1766	129	7.72
5	Sand	7.23	38	4940	3550	307	181	510	42	732	1491	132	6.73
6	Sand	7.37	30	4380	3140	315	143	385	43	648	1180	166	5.55
7	Limestone	7.54	28	3620	2570	202	126	350	23	510	1008	176	5.22
8	Limestone	7.36	32	2990	2540	247	103	375	23	531	1050	127	5.26
9	Limestone	7.14	28	3800	2690	211	157	398	23	560	1026	178	5.64
10	Limestone	7.19	27	3620	2560	213	170	370	24	533	1070	132	5.22
11	Limestone	7.24	25	3670	2610	211	164	400	22	542	1057	161	5.53
12	Limestone	7.18	25	3620	2590	202	165	384	22	538	1055	132	5.35
13	Limestone	7.18	26	3620	2590	176	187	369	22	536	1043	144	5.10
14	Limestone	7.18	24	3710	2720	214	165	380	22	550	1181	129	5.53
15	Limestone	7.61	25	3860	2740	221	172	401	23	569	1112	154	5.26
16	Limestone	7.28	25	3730	2660	237	130	389	23	551	1093	151	4.81
17	Limestone	7.26	24	3890	2760	211	186	380	25	572	1090	159	5.08
18	Limestone	7.56	31	4050	2880	240	182	385	28	598	1184	149	5.16
19	Limestone	7.27	42	4630	3820	320	126	535	44	685	1406	129	6.60
20	Limestone	7.15	33	4510	3230	416	143	471	36	666	1404	144	7.73
21	Limestone	7.4	27	4740	3410	261	184	525	40	703	1419	132	5.43
22	Limestone	7.68	31	4010	2880	328	133	410	29	597	1148	151	5.63
23	Limestone	7.41	31	4120	3070	320	156	460	32	637	1222	156	5.70
24	Limestone	7.38	26	4020	2870	317	136	390	27	596	1147	164	5.37
25	Limestone	7.27	31	3990	2870	285	132	445	21	595	1135	156	5.24
26	Limestone	7.29	25	3810	2720	235	158	390	26	566	1137	144	4.66
27	Limestone	7.27	24	4790	3460	320	156	515	39	715	1428	149	6.18
28	Sandstone	7.20	70	3130	2138	185	65	396	41	610	703	122	2.92
29	Sandstone	7.17	65	3460	2421	306	74	363	47	676	808	128	4.68
30	Sandstone	7.30	67	3340	2317	285	71	365	44	661	790	110	4.66
31	Sandstone	8.03	59	4040	2791	269	40	566	42	848	840	140	4.20
32	Sandstone	7.24	56	3750	2975	445	66	412	41	602	1260	134	6.02
33	Sandstone	7.20	65	3762	2508	362	68	369	44	638	1010	121	5.06

deposits which consist of red clays with intercalation of conglomeratic and sandy levels produced after the post-Cretaceous erosion (Bouaziz 1995; Benton *et al.* 2000). The thickness of these sand deposits increases from 25 to 80 m towards the sea. They are characterized by fine granulometry and permeability ranging from 2×10^{-5} to 4×10^{-4} m/s.

Hydraulic continuity between the CI and the Jeffara aquifer has been demonstrated through several hydrodynamic and isotopic studies (Gonfiantini *et al.* 1974; Mamou 1990; OSS 2003; Abidi 2004; Trabelsi *et al.* 2009). Hydraulic contact between the CI and Jeffara aquifers is suggested by the differences in hydraulic heads. The hydraulic heads of the CI aquifer indicate west–east flow (figure 4), in the direction of El Hamma–Chenchou region, with the hydraulic head of about 200 m (OSS 2003). On the other hand, the Jeffara aquifer shows a general southwest–northeast flow from the Matmata relief and El Hamma region towards the Mediterranean Sea, in accordance with the plain structure (figure 4). Near El Hamma faults, the hydraulic head is around 50 m, which is explained by the rise of CI groundwater through El Hamma faults (figure 2) assuring 2.12 m³/s recharge of the Jeffara aquifer (Mamou and Kassah 2002).

In Matmata region, Turonian and Senonian outcrops facilitate recharge of the Jeffara aquifer, estimated at 0.96 m³/s (Mamou and Kassah 2002). Discharge amounts to 5.25 m³/s, including artificial discharge by pumped wells (4.53 m³/s), the rest flows naturally into the Gulf of Gabes. Balance deficit is about 2 m³/s.

5. Analytical methods

A representative set of samples was collected from 33 active water supply boreholes/wells penetrating different lithological units in the Jeffara and the CI aquifers, during May 2009 (table 1 and figure 1). Temperature, electrical conductivity and pH were measured in the field. Samples of groundwater were kept in a refrigerator upon collection. Major and minor element determinations were carried out after filtering of samples through 0.45 μm filter. Geochemical analyses were carried out in the 'laboratoires du Groupe Chimique de Gabès'. Calcium and magnesium dosing was carried out by titration with EDTA. Sodium and potassium were measured using a flame photometer. Chloride and sulphate concentrations were determined using the Mohr and gravimeters methods, respectively. The total alkalinity (as HCO_3) was determined by titration with 0.01 or 0.1 M HCl and methyl orange as indicator. Strontium and duplicate analyses were

done (except for HCO_3) in the 'Institut Superieur des Sciences et Techniques des Eaux de Gabès, Tunisia' using HPLC Bishoff Lanbda 1010 type and an ionic liquid chromatography Metrohm 850 Professional IC type equipped with auto sampler, 858 Professional Sample Processor Metrohm type. Charge balance for all samples including strontium data is less than 5%.

6. Results and discussion

6.1 *Physico-chemical data*

Samples collected from the CI are characterized by high temperature varying from 56° to 70°C. Considerably lower temperature, ranging from 23° to 30°C was detected in the Miocene horizon, with the exception of one well (No. 9), where measured temperature was 37.8°C. Samples collected from limestone level of the Jeffara display an intermediate position between 24° and 41.6°C; while temperature of the Jeffara groundwater varies widely from 23° to 42°C. Independent of the borehole depth, the water temperature is the highest in the El Hamma region, which points to some inflow of groundwater from the CI aquifer through the network's most developed fault of the plain (figure 4).

The conductivity of CI groundwater samples ranges from 3130 to 4040 μS/cm. Conductivity of the Jeffara aquifer varies between 2990 and 6160 μS/cm. The highest values are

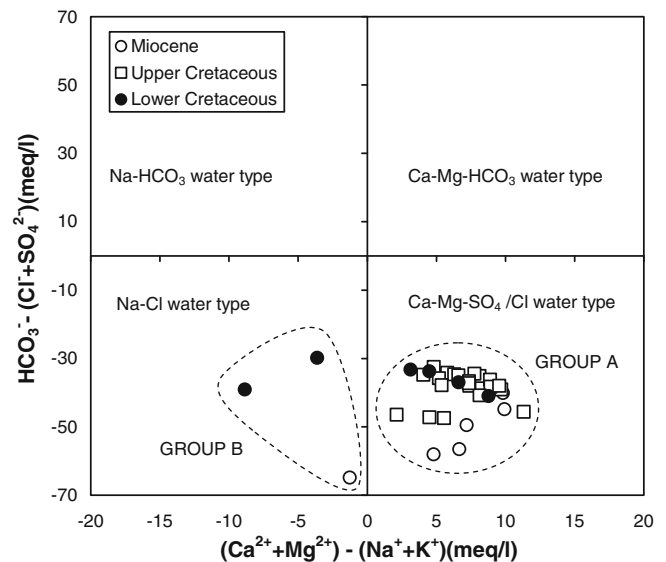

Figure 5. Chadha diagram showing the water type of the groundwater samples. Two sub-groups are identified in the Ca–Mg–SO₄/Cl water type.

measured in samples from the Miocene sands and limestone of El Hamma region. The salinity of Miocene sands aquifer in northern Gabes increases with time (Charfi 2004). High groundwater abstraction in this region to ensure industrial needs including water for phosphate treatment, leads to formation of the depression cone, which facilitates leakage of saline water from the local shallow saline drainage aquifer formed by return flow irrigation. In the El Hamma region, the salinity of groundwater is abnormally high, suggesting that saline water originated from Chott El Fedjaj.

6.2 *Water types*

Chemical composition of the analysed groundwater samples is plotted on the Chadha diagram (Chadha 1999), which is a somewhat modified version of the Piper diagram and the expanded Durov diagram; the difference is that the two equilateral triangles are omitted (Chadha 1999). The plot of the CI and Jeffara groundwater samples in the Chadha diagram (figure 5) presents two groups; the alkaline earth-rich group (Group A) and the alkali metals-rich group (Group B). The first group, which comprised the majority of the analysed samples, showed that the alkaline earth (Ca+Mg) exceeded the alkali metals (Na+K) and that the strong acids (Cl+SO$_4$) exceeded the weak acid (HCO$_3$). The second group, which included only two samples from the CI and a single sample from the Miocene aquifer, revealed that (Na+K) was superior to (Ca+Mg) and the strong acids (Cl+SO$_4$) exceeded the weak acid (HCO$_3$). Group A plots on the field of the Ca–Mg–SO$_4$/Cl water type and group B, on the field of Na–Cl water type.

6.3 *Major ions geochemistry*

Dominant cations are mainly sodium and calcium, while dominant anions are sulphate and chloride. Bivariate diagrams of major elements are used in order to separate different mechanisms that contribute to groundwater salinization. In particular, sodium is positively correlated with chloride and sulphate with calcium (figure 6a, b). These relations indicate the possible dissolution of halite, gypsum and/or anhydrite-bearing rocks relatively abundant, especially in the shallow levels of the Jeffara groundwater (less than 100 m depth).

However, the plot of SO$_4$ versus Ca (figure 6b), drawn for the Jeffara groundwater samples, shows a relative Ca depletion, probably related to additional source of sulphate releasing from evaporites horizons, abundant in the sandy Miocene formation.

Analyses of minor elements indicate significant enrichment of strontium (from 2.92 to 7.73 mg/l). Sr shows a linear relationship with both SO$_4$ and Ca (figure 7a, b). Probable sources of strontium are celestite (SrSO$_4$) dissolution and/or dissolution of gypsum/anhydrite containing trace concentrations of this element. Indeed, waters with high strontium and sulphate concentrations are undersaturated with respect to celestite, making dissolution possible (Edmunds *et al.* 1997; Kamel *et al.* 2005).

In the Jeffara waters, SI$_{celestite}$, ranges from -0.953 and -0.385 (table 2). None of the waters are undersaturated with respect to celestite, making the second assumption more plausible.

Mean SI$_{celestite}$ (-0.607), close to mean SI$_{gypsum}$ (-0.455), reinforce trace inclusion of celestite in gypsum.

Although Jeffara waters are unsaturated with respect to strontianite (SrCa)CO$_3$, with a mean
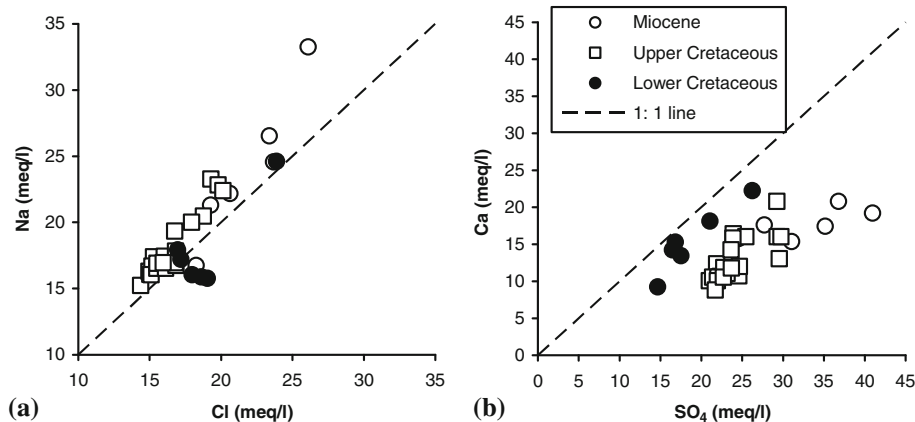

Figure 6. Bivariate diagrams between major elements: (**a**) Na/Cl and (**b**) Ca/SO$_4$, highlighting positive correlation between sodium and chloride and calcium deficiency.
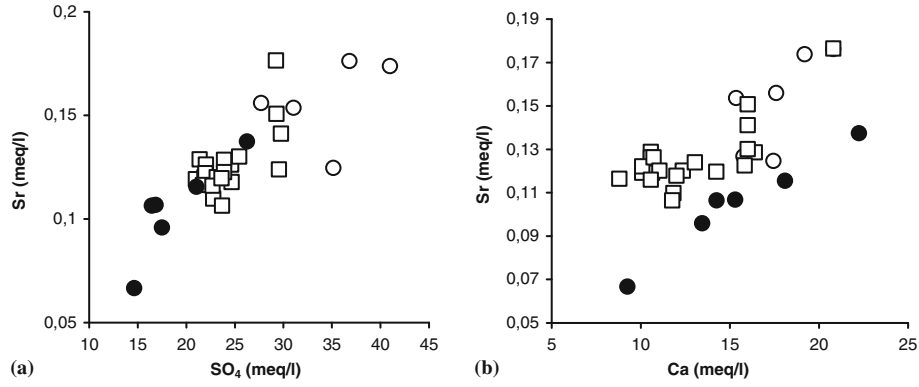
Figure 7. Relationships between (**a**) Sr/SO$_4$ and (**b**) Sr/Ca. Strontium is positively correlated with both sulphate and calcium, probably reflecting its association with gypsum.

Table 2. *Saturation indices of main minerals involved in sulphate geochemistry.*

Map no.	SI$_{Halite}$	SI$_{Calcite}$	SI$_{Dolomite}$	SI$_{celestite}$	SI$_{strontianite}$	SI$_{Gypsum}$	SI$_{Anhydrite}$	SI$_{Mirabilite}$	SI$_{Thenardite}$
1	−5.025	0.131	0.344	−0.551	−1.323	−0.283	−0.500	−4.618	−5.546
2	−4.861	0.026	0.066	−0.385	−1.330	−0.215	−0.432	−4.314	−5.241
3	−5.166	0.007	0.084	−0.505	−1.343	−0.341	−0.558	−4.831	−5.760
4	−4.999	0.384	0.667	−0.392	−0.998	−0.197	−0.414	−4.538	−5.465
5	−5.123	−0.032	0.081	−0.478	−1.337	−0.361	−0.578	−4.741	−5.670
6	−5.286	0.257	0.544	−0.602	−1.133	−0.398	−0.616	−5.056	−5.986
7	−5.419	0.288	0.745	−0.629	−0.934	−0.594	−0.811	−5.148	−6.079
8	−5.373	0.053	0.098	−0.618	−1.255	−0.496	−0.714	−5.078	−6.008
9	−5.328	−0.089	0.065	−0.611	−1.296	−0.591	−0.809	−5.056	−5.986
10	−5.381	−0.170	−0.066	−0.634	−1.415	−0.575	−0.793	−5.105	−6.035
11	−5.340	−0.038	0.188	−0.613	−1.253	−0.583	−0.801	−5.042	−5.972
12	−5.360	−0.202	−0.118	−0.624	−1.412	−0.599	−0.817	−5.074	−6.004
13	−5.379	−0.221	−0.045	−0.649	−1.393	−0.663	−0.881	−5.115	−6.045
14	−5.359	−0.199	−0.138	−0.583	−1.427	−0.541	−0.759	−5.041	−5.971
15	−5.321	0.317	0.898	−0.628	−0.941	−0.556	−0.773	−5.027	−5.957
16	−5.345	0.022	0.157	−0.657	−1.307	−0.515	−0.732	−5.043	−5.973
17	−5.341	−0.030	0.256	−0.650	−1.283	−0.583	−0.800	−5.085	−6.014
18	−5.320	0.280	0.812	−0.627	−1.024	−0.509	−0.726	−5.047	−5.977
19	−5.127	0.028	0.029	−0.488	−1.302	−0.345	−0.562	−4.705	−5.634
20	−5.196	0.069	0.049	−0.438	−1.302	−0.253	−0.471	−4.845	−5.774
21	−5.125	0.074	0.371	−0.575	−1.251	−0.437	−0.655	−4.726	−5.655
22	−5.293	0.542	1.066	−0.602	−0.858	−0.388	−0.606	−5.012	−5.941
23	−5.219	0.269	0.599	−0.590	−1.116	−0.391	−0.609	−4.900	−5.829
24	−5.315	0.269	0.543	−0.620	−1.137	−0.400	−0.618	−5.052	−5.982
25	−5.258	0.096	0.231	−0.628	−1.275	−0.443	−0.661	−4.934	−5.864
26	−5.337	−0.002	0.265	−0.681	−1.341	−0.529	−0.746	−5.052	−5.982
27	−5.126	0.085	0.232	−0.521	−1.273	−0.350	−0.567	−4.743	−5.672
28	−5.277	−0.194	−0.473	−0.953	−1.618	−0.714	−0.931	−5.154	−6.084
29	−5.280	−0.010	−0.266	−0.750	−1.449	−0.498	−0.715	−5.226	−6.156
30	−5.285	0.028	−0.181	−0.750	−1.383	−0.526	−0.743	−5.220	−6.150
31	−4.994	0.797	1.143	−0.784	−0.634	−0.539	−0.757	−4.817	−5.746
32	−5.290	0.179	−0.098	−0.551	−1.328	−0.229	−0.446	−4.973	−5.903
33	−5.304	0.040	−0.273	−0.665	−1.446	−0.364	−0.582	−5.134	−6.063

SI$_{strontianite}$ equal to −1.136, calcium can be substituted by strontium in gypsum, explaining the positive correlation between Sr and Ca (figure 7b).

Saturation state of the waters with respect to halite, gypsum/anhydrite, mirabilite/thenardite, celestite and strontianite were performed using
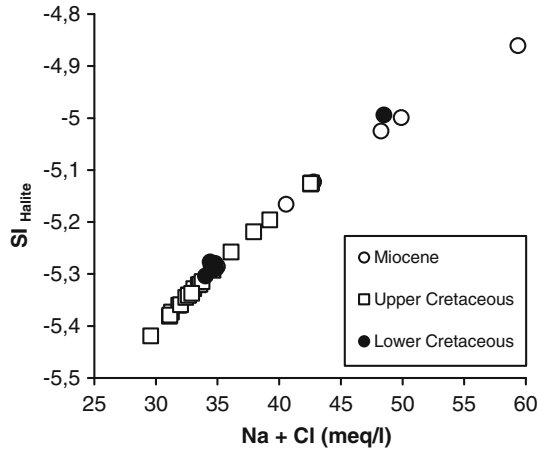
Figure 8. Plot of (Na + Cl) versus SI $_{Halite}$. Undersaturation with respect to halite, reinforced halite dissolution in the three studied aquifers.

WateqF subroutine program (Plummer *et al.* 1992).

A saturation index of zero indicates that ion activity and solubility products are equal, and that thermodynamic equilibrium exists with the solid phase. A negative or positive index indicates undersaturation or oversaturation, respectively (Gemici and Filiz 2001).

Under ambient temperature, all water samples collected in both CI and Jeffara groundwaters are unsaturated with respect to halite ($-5.419 <$ IS < -4.861) (table 2). Figure 8 shows a positive correlation between SI$_{halite}$ and (Na + Cl), reinforcing halite dissolution in the referred aquifers.

The origin of sulphate, which is the most dominant cation in 90% of water samples, may be evidenced using gypsum/anhydrite and mirabilite/thenardite couples.

Sulphates may originate from either the dissolution of gypsum (CaSO$_4$, 2(H$_2$O))/anhydrite (Ca SO$_4$) in which they are associated with calcium, or the dissolution of mirabilite (Na$_2$SO$_4$, 10(H$_2$O))/thenardite (Na$_2$SO$_4$) when they are associated with sodium.

Figure 9(a, b) shows linear positive correlation between SI of those phases and ion concentrations. Thus, the dissolution of these evaporites probably occurs in the aquifer, first because those phases are present and secondly because there are favourable conditions with their negative saturation indices.

6.4 *Water composition evolution under variable temperature conditions*

The Jeffara recharge by the deep geothermal CI is supposed to occur in the area of El Hamma Chenchou at the intersection of a network of east–west and north–south fractures.

In order to model the evolution of water chemistry more precisely, the effect of variable temperature on mineral–water equilibria has been considered.

Plots of wellhead temperature versus several elements (Mg, Na, Ca, K, Sr, Cl, HCO$_3$ and SO$_4$) (figure 10) showed that concentrations of Mg, Sr and SO$_4$, increase with wellhead temperature, whereas K decreases in Miocene and Upper Cretaceous non-thermal samples. Sodium, Ca and Cl water contents, lie within the same range for both geothermal and non-thermal waters. Deep geothermal groundwaters generally contain low
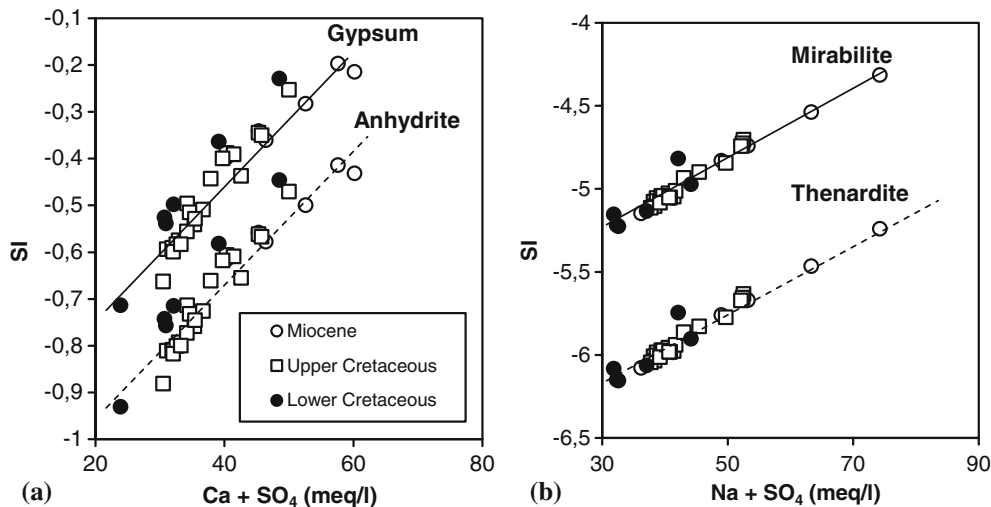

Figure 9. Minerals saturation indices (SI)/representative species relationship; (**a**) SI/(Ca + SO$_4$) and (**b**) SI/(Na + SO$_4$).
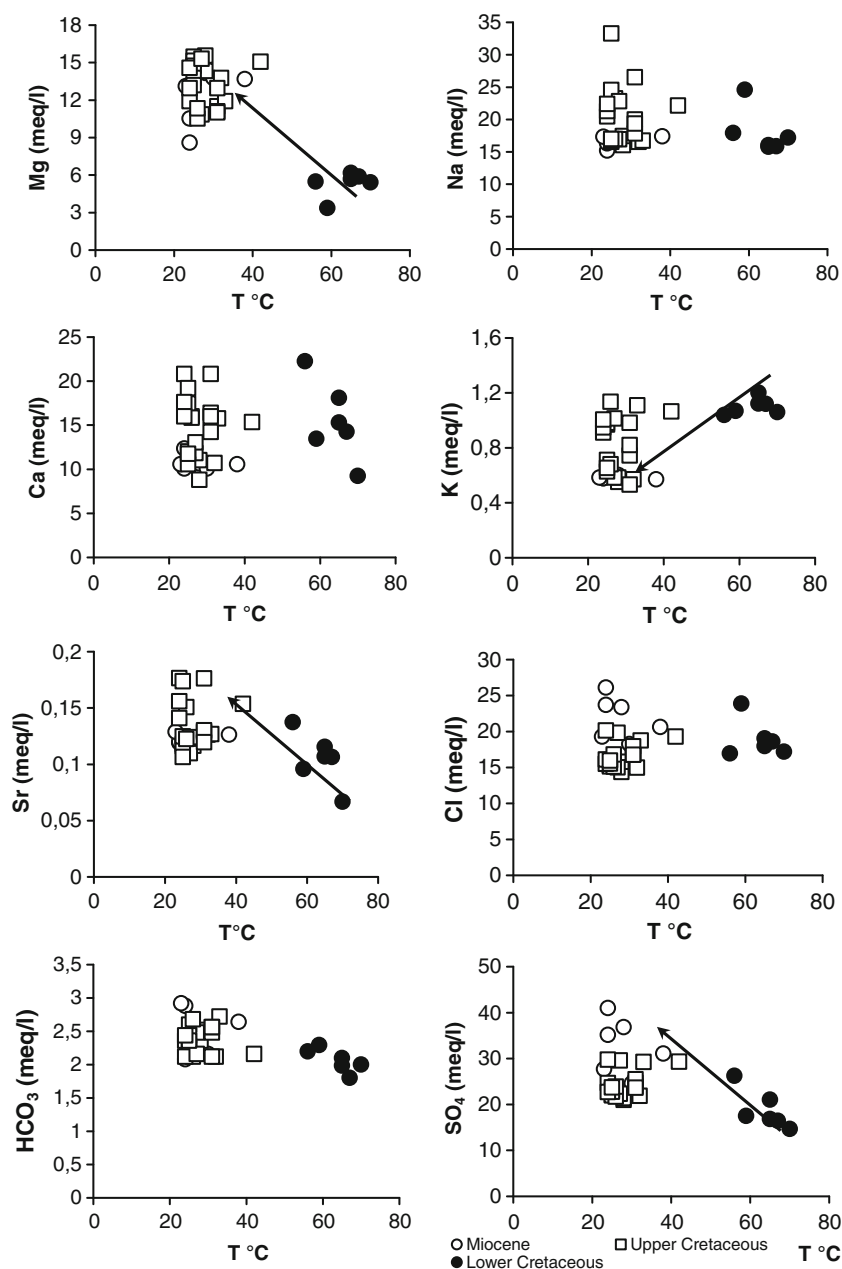
Figure 10. Major elements/temperature relationship: Mg, Sr and SO_4 increase with temperature, whereas K decreases in Miocene and Upper Cretaceous non-thermal samples. Sodium, Ca, Cl and HCO_3 lie within the same range for both geothermal and non-thermal waters.

SO_4 content (<50 mg/l) (Nicholson 1993). Sulphate content of CI water is quite high (703–1260 mg/l) in the study area. High sulphate concentration could be explained by buried gypsum dissolution within the lower Senonian formation.

The relationship between Ca/SO_4 ratio and wellhead temperature of the geothermal and non-geothermal waters samples is shown in figure 11. Taking into consideration the distinctive values of Ca/SO_4 ratio of lower Cretaceous water (0.6 to 0.9) and Miocene water (0.2 to 0.4), these two mass waters could be assumed to be two

end-members representing deep geothermal and shallow non-geothermal waters, respectively. Waters sampled from Upper Cretaceous aquifer are plotted on two subgroups on intermediate position between Miocene and Lower Cretaceous waters. Upper cretaceous subgroup 1 displays the same Ca/SO_4 ratio value of geothermal water resulting probably from the major contribution of CI groundwater, recharging the Jeffara aquifer. Samples within the subgroup 1 are placed between El Hamma–Chenchou–Gabes axis and Matmata–Mareth,
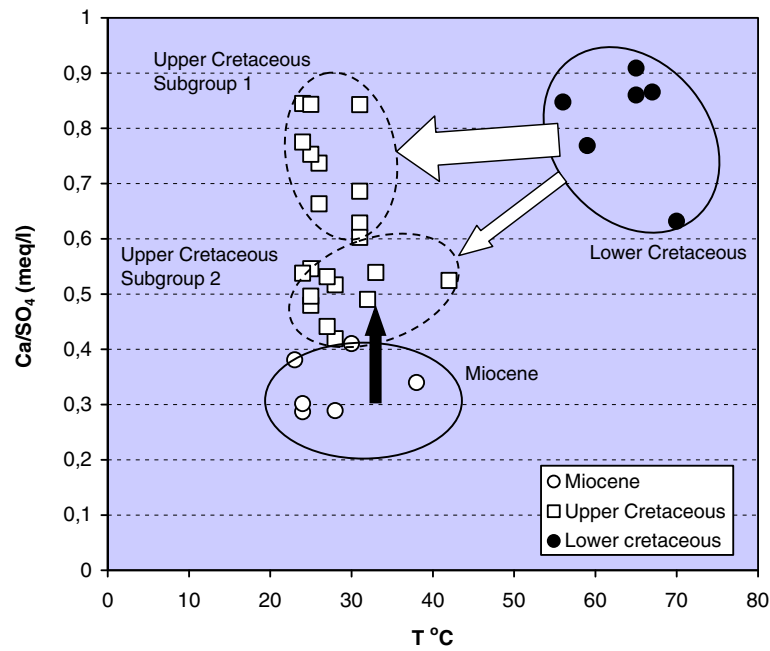
Figure 11. Ca/SO$_4$ versus water temperature, showing two lower Cretaceous and Miocene end-members. Upper Cretaceous presents two sub-groups related to the CI rate contribution, recharging the fissured limestone aquifer.
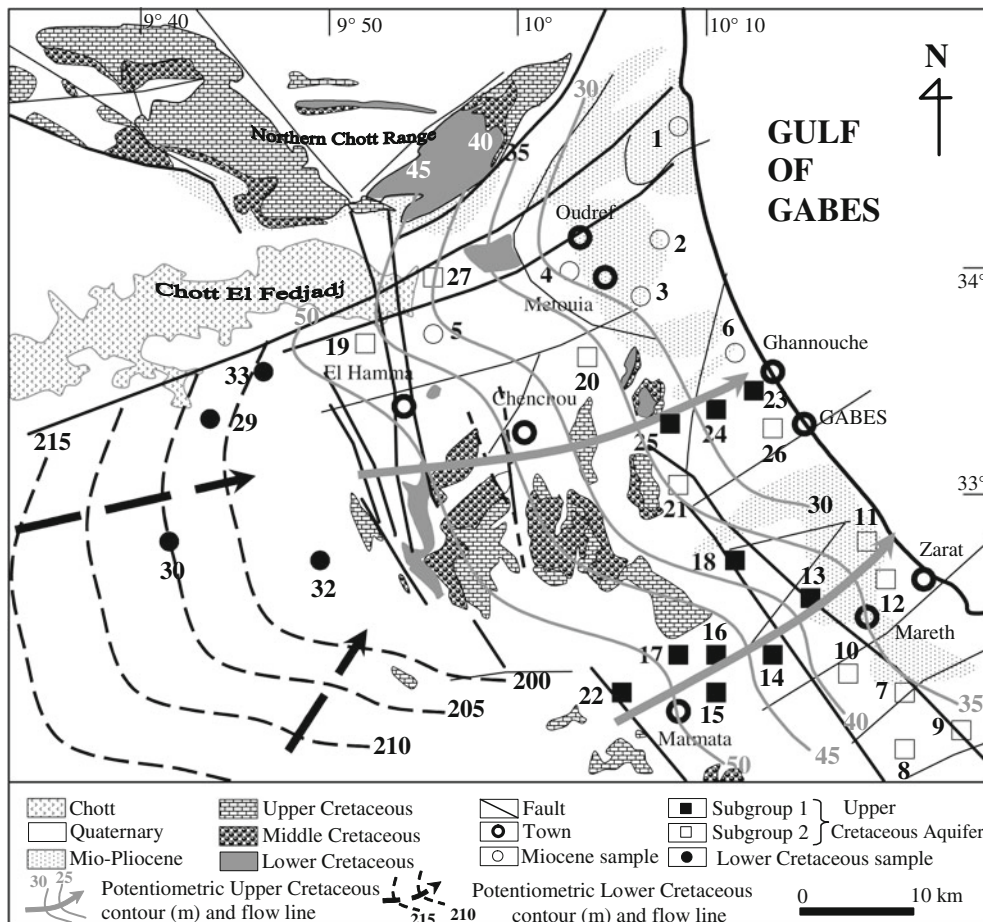

Figure 12. Potentiometric Lower and Upper Cretaceous surface contour showing preferential flow axes in relation to major faults in the study area.

where the fault system is the most significant in the region.

Upper Cretaceous subgroup 2 occupies an intermediate position between the two end-members, reflecting the mixing ascent geothermal and surface water. The northern Chott range and the south Matmata–Mareth axis where fissured limestones of Senonian level outcrop, constitute the preferential local recharge by the downward rainy events from Matmata and Dahar reliefs (figure 12).

The mean concentration compounds in water representing the two end-members (Lower Cretaceous and Miocene) give a mixing ratio for the intermediate Upper Cretaceous water (using AquaChem 3.70/Mix samples) of about 40% for gypsum dissolution ($CaSO_4$). The same range computed contributions using isotopic model, varies from 29% to 53% (Trabelsi *et al.* 2009).

7. Conclusion

The structure 'in horst and graben', which is the main feature in the compartmentalization of the Jeffara aquifer, is mainly responsible for the hydraulic continuity between Turonian, Senonian and Miocene aquifer levels.

The faulted geological structure of the Jeffara aquifer system in the El Hamma region has played a major role in its recharge by the CI geothermal aquifer.

Piezometry, water temperatures as well as chemical and isotopic compositions, confirm the hydraulic continuity between these two aquifers (Trabelsi *et al.* 2009).

The hydrochemical characteristics of the Jeffara groundwater comprise two water types resulting mainly from evaporites dissolution. The Ca–Mg–SO_4–Cl main water type highlighted the predominance of the gypsum dissolution, largely spread into subsurface and deep in various forms; while, the second Na–Cl water type results from halite dissolution, locally outcropping as a diapir, in the northern Chott Chain (Hadifa Mn.) and/or restricted contamination by saline lakes brine, in the vicinity of oases.

Bivariate diagrams of major elements confirm the dissolution of evaporites as a potential origin of the Jeffara water salinization.

The computed SI values showed that groundwater in the Jeffara aquifer was largely undersaturated with respect to halite, thenardite and mirabilite, to a lesser extent, with respect to anhydrite and gypsum, indicating possible dissolution of these minerals. These eventual dissolutions were confirmed by strong positive relationships between SI and ions resulting from the referred dissolutions for all three aquifers.

Solubility of anions and cations changes from the CI to the Jeffara aquifers (sulphate, strontium and magnesium increase, potassium decreases and sodium, calcium, chloride and bicarbonates show no content variation) without notable change in the water type. The constancy of water type for all the three aquifers, reflects the CI large contribution and/or the predominance of evaporate dissolution as the main process of water salinization. In the study area, abundant surface and buried gypsum reinforce this supposition.

The mixing rate inferred from Ca/SO_4 versus temperature shows that CI-contribution recharging upper fissured limestone aquifer occurs mainly between El Hamma–Chenchou and Mareth regions. Evaporite dissolution can be a significant process on a regional scale in carbonate aquifers and give rise to early high permeability groundwater flow paths that influence later aquifer development by the 'normal' process of carbonate dissolution (Gunn *et al.* 2006).

References

Abidi B 2004 *Caractéristiques hydrodynamiques et géochimiques de la Jeffara de Gabès*; Tech. Doc. DGRE, Tunis, p. 198.

Ben Ayed N 1986 *Evolution tectonique de l'avant pays de la chaine alpine de Tunisie du début du Mésozoique à l'actuel*; Thesis Univ. Paris Sud, Centre d'Orsay, France, p. 286.

Ben Baccar B 1982 Contribution à l'étude hydrogéologique de l'aquifère multicouche de Gabès Sud. Doctorat Thesis Paris Sud France, p. 115.

Ben Ouezdou H 1983 *Etude morphologique et stratigraphique des formations quaternaires dans les alentours du Golfe de Gabès*; Doctorat Thesis, Faculté des Sc. Humaines et Sociales, Tunis, p. 216.

Benton M, Bouaziz S, Buffetaut E, Martil D, Ouaja M, Soussi M and Trueman C 2000 Dinosaurs and other fossil vertebrates from fluvial deposits in the Lower Cretaceous of southern Tunisia; *Palaeogeogr. Palaeoclimatol. Palaeoecol.* **157** 227–246.

Bouaziz S 1995 Etude de la tectonique cassante dans la plate-forme et l'Atlas saharien (Tunisie Méridionale): Evolution des paléochamps de contraintes et implications géodynamiques; Thesis, University of Tunis II. Faculty of Sciences of Tunis, Tunisia, p. 485.

Bouaziz S, Barrier E, Soussi M, Turki M M and Zouari H 2002 Tectonic evolution of the northern African margin in Tunisia from paleostress data and sedimentary record; *Tectonophys.* **357** 227–253.

Bouri S, Makni J and Ben Dhia H 2008 A synthetic approach integrating subsurface and surface data for prospecting

deep aquifers: the southeast Tunisia; *Environ. Geol.* **54** 1473–1484.

Chadha D K 1999 A new diagram for geochemical classification of natural waters and interpretation of chemical data; *Hydrogeol. J.* **7** 431–439.

Charfi S 2004 Contribution à l'étude hydrogéologique, hydrochimique et isotopique de la nappe de la Jeffara de Gabès; Master degree, Laboratory of Radio-Analysis and Environment, National School of Engineers of Sfax (Tunisia), p. 91.

DGRE 2009 Direction Générale des Ressources en Eau. Annuaire d'exploitation des nappes profondes de la Tunisie; DGRE Tunis, p. 373.

Edmunds W M, Shand P, Guendouz A H, Moula A, Mamou A and Zouari K 1997 Recharge characteristics and groundwater quality of the Grand Erg Oriental basin; Tech. Rep. Wd/97/46R, Vienna, p. 92.

Gabtni H, Mickus K L, Zouari H and Turki M M 2006 The location and nature of the Telemzan High-Ghadames basin boundary in southern Tunisia based on gravity and magnetic anomalies; *J. African Earth Sci.* **44** 303–313.

Gemici U and Filiz S 2001 Hydrogeochemistry of the Cesme geothermal field, western Turkey; *J. Volcanol. Geotherm. Res.* **110** 171–187.

Gonfiantini R, Conrad G, Fontes J C, Sauzy G and Payne B R 1974 Etude isotopique de la nappe du Continental Intercalaire et de ses relations avec les autres nappes du Sahara septentrional; In: *Isotope techniques in groundwater hydrology*, Proc. Symp. IAEA Vienna I, pp. 227–241.

Guendouz A, Moula A S, Edmunds W M, Zouari K, Shand P and Mamou A 2003 Hydrogeochemical and isotopic evolution of water in the complexe terminal aquifer in the Algerian Sahara; *J. Hydrol.* **11** 483–495.

Gunn J, Bottrell S H, Lowe D J and Worthington S R H 2006 Deep groundwater flow and geological processes in limestone aquifers: Evidence from thermal waters in Derbyshire, England, UK; *Hydrogeol. J.* **14** 868–881.

Kamel S, Dassi L, Zouari K and Abidi B 2005 Geochemical and isotopic investigation of the aquifer system in the Djerid–Nefzaoua basin, southern Tunisia; *Environ. Geol.* **49** 159–170.

Kettata M, Hamzaoui F, Gueddari M, Bouhlila R and Ribeiro L 2009 Hydrochemical and statistical study of groundwaters in Gabes-south deep aquifer (south-eastern Tunisia); *Phys. Chem. Earth* **36** 187–196.

Kinsman D J 1966 Gypsum and anhydrite of recent age, Crucial Coast, Persian Gulf; Proc. 2nd Salt Symp. Northern Ohio; *Geol. Soc.* **1** 302–326.

Mamou A 1990 *Caracteristiques et évaluation et gestion des ressources en eau du Sud Tunisien*; Thesis Univ. Paris Sud France, p. 426.

Mamou M and Kassah A 2002 *Eau et développement dans le sud tunisien; Cahiers du CERES*, série géographique no. 23, Tunis, p. 268.

Mekrazi A F 1975 *Contribution à l'étude géologique et hydrogéologique de la région de Gabès Nord*; Thesis University of Bordeau I, France, p. 160.

Mhamdi A, Dhahri F, Gouasmia M, Inoubli N, Soussi M, and Ben Dhia H 2011 Groundwater investigation in the southern part of Gabes using resistivity sounding, southern Tunisia; *Arab J. Geosci.* (published online), p. 14.

Nicholson K 1993 *Geothermal fluids: Chemistry and exploration techniques* (Heidelberg, Berlin: Springer-Verlag), p. 262.

OSS (Observatoire du Sahara et du Sahel) 2003 *Système aquifère du Sahara septentrional. Une conscience de bassin*; Vol. II. Hydrogéologie. Observatoire du Sahara et du Sahel, p. 322.

Plummer L N, Prestmon E and Parkhurst D L 1992 An interactive code (netpath) for modelling net geochemical reaction along a flow path; Techniques of water resources investigations of US Geological Survey, p. 91.

Rouatbi R 1967 *Contribution à l'étude hydrogéologique du karst enterré de Gabès*; Sud. Thesis Doctorat Univ. Montpellier, France, p. 224.

Swezey C 2003 The role of climate in the creation and destruction of continental stratigraphic records: An example from the northern margin of the Sahara desert; *SEPM (Society of Sedimentary Geology), Spec. Publ.* **77** 207–225.

Trabelsi R, Kassem A, Zouari K and Rozanski K 2009 Quantifying regional groundwater flow between Continental Intercalaire and Djeffara aquifers in southern Tunisia using isotope methods; *Environ. Geol.* **58** 171–183.